Research on the Detecting Effectiveness of On-site Lightning Impulse Test for GIS Equipment with Insulation Defects

Tao Wen
State Key Laboratory of Electrical Insulation and Power Equipment, Xi'an Jiaotong University
Xi'an, 710049, P.R. China
Tokushima University, 2-1 Minami-Josanjima
Tokushima 770-8506, Japan

Qiaogen Zhang, Jingtan Ma, Xuandong Liu, Zhicheng Wu, Lingli Zhang, Junping Zhao
State Key Laboratory of Electrical Insulation and Power Equipment, Xi'an Jiaotong University
Xi'an, 710049, P.R. China

Naoyuki Shimomura
Tokushima University, 2-1 Minami-Josanjima
Tokushima 770-8506, Japan

and **Weijiang Chen**
State Grid Corporation of China, 86 West Chang'an Street
Beijing, 100031, China

ABSTRACT

On-site lightning impulse (LI) test waveform, restricted by the large load capacitance and impulse generator's inherent inductance, has a long wavefront time T_f compared with standard LI, called non-standard LI. The non-standard LI test has been carried out in the field. But its insulation defect detecting effectiveness is not clear. In this paper, a generating system of impulses with different waveform parameters, including double-exponential impulses with different wavefront times in the range of 0.08 ~ 23.5 μs and an oscillating LI with wavefront time around 10 μs, was established. The insulation characteristics of SF_6 gas gap with highly inhomogeneous electric field under impulses with different waveform parameters were investigated. Experimental results show that the insulation defects detecting effectiveness of oscillating LI with long T_f around 10 μs is lower than that of standard LI. T_f plays an important role in the insulation defects detection. With T_f increases, the 50% breakdown voltages for rod-plane gaps have an increased trend. The V-t curve presents a U-shape. Prospective voltage is introduced to evaluate the insulation defects detecting effectiveness. The prospective voltage-time characteristics confirm the conclusion that with the increase of impulse voltage T_f, the detection effectiveness for GIS insulation is reduced. The gap distance has influence on the shape of V-t curve. With distance increase, the 50% breakdown voltage of the gap is more sensitive to the wavefront time T_f and voltage rise rate dU/dt. Corona stabilization effect is not just in relationship with the rise rate of impulse, but also with electrode structure and gas pressure. The critical dU/dt for corona stabilization is calculated for different rod-plane gaps.

Index Terms — **Gas-insulated metal-enclosed switchgear (GIS), on-site test, lightning impulse (LI), wavefront time, 50% breakdown voltage, voltage-time characteristic, prospective voltage, detecting effectiveness.**

1 INTRODUCTION

GAS-insulated metal-enclosed switchgear (GIS) has developed rapidly since the mid-1960s [1-5]. Compared with traditional air insulated switchgear, the GIS makes the bus, isolating switch, circuit breaker, lightning arrester and many other devices all safely sealed away in a benign environment of dry, noncorrosive, high dielectric strength gas SF_6 [6]. It has many advantages such as reliability, compaction, long maintenance cycle, and small impact on the environment,

Manuscript received on 11 August 2017, in final form 10 January 2018 accepted 18 January 2018.d Corresponding author: Q. Zhang.

DOI: 10.1109/TDEI.2018.006961

which have led to it being widely used in electrical power systems [7-8].

However, under such condition, series of serious breakdown failures still occur in GIS [9-10]. One might reasonable wonder what fundamentally cause the insulation accidents. As we all known that quasi-uniform electric field is used in the designing of GIS to improve the electrical strength for SF_6 is sensitive to the electric field. For a GIS well designed, it does not fail unless a defect of some sort is present, which implies an inhomogeneous electric field appears in the system. The factory test on shipping units does not cover possible defects due to transportation, storage, environment, final assembly and mechanical testing on-site. With the dielectric test on-site those defects which could cause an outage of the system during service must be found. It is important to point out, that on-site testing is not a repetition of a type test, with which the conformity of the design has been proven. It is also not a replacement or supplement of the routine test in the factory. Therefore the aim of the dielectric test on-site is to prove the integrity of the system after shipping, storage, assembly, repair, extension and further tests, before it is energized. It is the final step of the long process of quality control and quality assurance [6].

Lightning impulse (LI) test, as one kind of the on-site withstand voltage tests, is particularly sensitive to abnormal field configurations, e.g., damaged electrodes, and is recommended in IEC 62271-203 for voltage classes of 245 kV and above [11-12], should be carried out to ensure sufficient insulation capability under overvoltage and detect any defects resulting from field installation. According to the IEC 60060-1 (2010) "High-voltage test techniques" standard, the standard LI is a smooth full lightning impulse voltage with a front time of 1.2 μs ± 30%, a time to half-value of 50 μs ± 20% [13]. But it is difficulty in generating a lightning impulse waveform that meets the standard due to factors such as the increase in series inductance attributable to the longer and larger test circuit and the increased capacitance of the equipment to be tested [14]. In order to carry out the impulse voltage test, based on the existing traditional open impulse equipment, IEC has also proposed a non-standard LI test in which the T_f of the impulse voltage waveform can be as much as 8 μs, or, when using oscillating LI (OLI) voltages, as much as 15 μs. But the insulation defect detecting effectiveness is not clear, compared with standard LI test, which maybe one reason for the failures of GIS which has passed the on-site withstand voltage test successfully.

In this paper, in order to obtain the defect detecting effectiveness of non-standard LI, the breakdown characteristics of SF_6 with highly inhomogeneous electric field under impulses with different waveform parameters were studied.

2 EXPERIMENTAL SETUP AND METHOD

2.1 EXPERIMENTAL SETUP

An impulse generating system based on a fully enclosed, oil-insulated Marx generator and a simulated GIS bus is established, as shown in Figure 1. The Marx generator and simulation GIS bus are separated by dielectric spacers and a basin-type insulator. By immersing the Marx generator in oil, the generator can be made very compact, thereby lowering inductance, which affects the front time of the output waveform. The generator could generate double-exponential impulses with wide range T_f in the range of 0.08 ~ 23.5 μs and wave tail time around 50 μs, including SLI, or an OLI with wavefront time around 10 μs and oscillation frequency around 25 kHz, as shown in Figure 2. A conical voltage sensor was used for the measurement of impulse waveforms. The calibrating results indicated that the response of the conical voltage senor can accurately measure the impulses with wavefront time from 80 ns to 23.5 μs accurately.

The electrode in Figure 3 was used to simulate local-field enhancement in GIS. The high voltage electrode of rod-plane electrode was a 0.5-mm-radius hemispherically capped stainless steel rod. The grounded plane was a 300-mm-diam Rogowski stainless steel electrode. The gap distance d could be adjusted 33, 45 and 60 mm in this experiment. The field nonuniformity factor f simulated by Ansoft was shown in Table 1. The test setup was installed in a chamber filled with SF_6 to absolute pressures in the range 0.3-0.6 MPa.

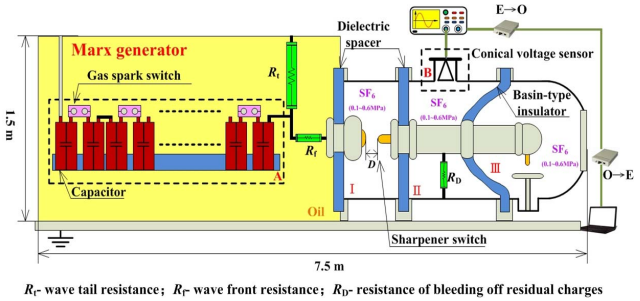

R_t- wave tail resistance; R_f- wave front resistance; R_D- resistance of bleeding off residual charges

Figure 1. Schematic diagram of impulse generating system.

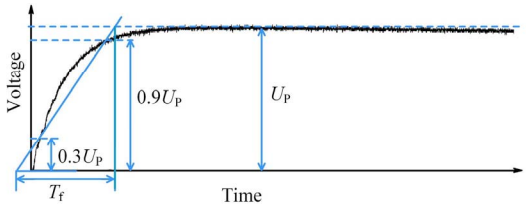

(a) double-exponential LI with T_f in the range 0.08 - 23.5 μs

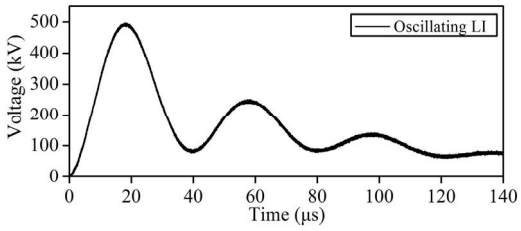

(b) OLI with T_f around 10 μs

Figure 2. Output impulse voltages with different waveform parameters.

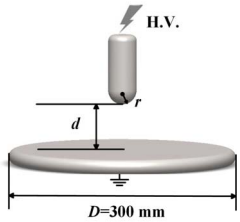

Figure 3. Configuration of rod-plane electrode.

Table 1. Field nonuniformity factor of rod-plane electrodes.

Parameters	Rod-plane electrodes		
r/mm	0.5		
d/mm	33	45	60
f	30.48	35.46	42.57

2.2 EXPERIMENTAL METHOD

In SF_6 highly inhomogeneous electric field, the breakdown voltage under positive polarity is lower than that under negative polarity. So the positive polarity voltage was used in this study. The waveforms were recorded using an oscilloscope (Tektronix DPO4104) with a bandwidth of 1 GHz and a sample rate of 5 Gs/s. Calibration results demonstrated that the response time of the measuring system was less than 5 ns and the uncertainty of divider ratio was less than 3%. The voltage-time characteristic of the rod-plane electrode system was obtained by applying impulse voltages of various amplitudes, and its 50% breakdown voltage by using the up-and-down method described in IEC 60060-1 [13].

Here, the prospective voltage value used in the calculation of 50% breakdown voltage, and the breakdown voltage value used in the voltage-time characteristic, should be clarified, which maybe cause some misunderstandings in the follow discussions of insulation defect detecting effectiveness. The 50% breakdown voltage is the prospective voltage value which has a 50% probability of producing a disruptive discharge on the test object. When calculating the 50% breakdown voltage (equal the mean value of the data obtained using up-and-down method), it should use the prospective voltage value, not the recorded breakdown voltage values.

For the used impulse waveforms, the breakdown may occur in the front, near the peak, or in the tail of the impulse. For breakdown occurs in the front of the impulse (breakdown time $T_b < T_f$), as shown in Figure 4a), the breakdown voltage is the peak value of the recorded waveform (If breakdown, the impulse will fast drop to zero from the breakdown point and the part after breakdown point cannot be recorded). But the prospective voltage is the peak value of the full waveform assumed that the test object is not breakdown. In this case, the prospective voltage is higher than the breakdown voltage. For breakdown occurs near the peak or in the tail of the impulse (breakdown time $T_b \geq T_f$), as shown in Figure 4b), the breakdown voltage is the peak value of the recorded waveform as well. In this case, the prospective voltage is equal to the breakdown voltage. The insulation defect detecting effectiveness using the impulse test is reflected in the value of the prospective voltage, i.e., the higher the prospective voltage the lower the effectiveness of defect detection.

The prospective voltage value U_p, not affected by the measured waveform, is the peak value of the impulse voltage stressed on the test object assumed that there is no disruptive discharge, calculated by the impulse voltage generator's charging level voltage U_L, levels N and output efficiency η ($U = U_L \cdot N \cdot \eta$). The double-exponential impulse's waveform function can be written as follows:

$$U(t) = U_m(e^{-at} - e^{-bt}) \quad (1)$$

where, U_m is the amplitude parameter, equals to The prospective voltage value U_p. a, b are waveform parameters, considered by the wave tail time and wavefront time respectively. When the breakdown time T_b and the breakdown voltage U_b are known, the prospective voltage value U can also be calculated by the stressed waveform function $U(t)$.

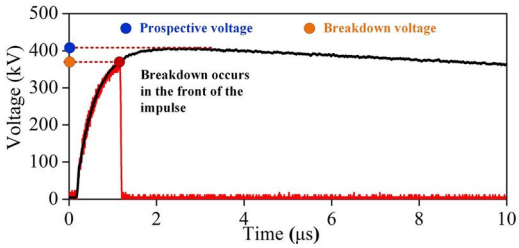

(a) breakdown occurs in the front

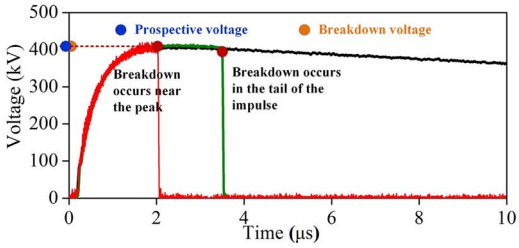

(b) breakdown occurs near the peak or in the tail

Figure 4. Definition of the prospective voltage and breakdown voltage in the article.

3 EXPERIMENTAL RESULTS AND DISCUSSION

3.1 THE EFFECTIVENESS OF OSCILLATING LI

Usually, a non-standard LI test for GIS in the field called oscillating LI test with long T_f is preferred for the easy obtained and high output efficiency η. The on-site oscillating LI test has been carried out in the Three Gorges hydropower station 550 kV GIS, especially in the Zhe-Fu ultra high voltage (UHV) GIS substation, in China. A typical waveform of the oscillating LI, as shown in Figure 2b), is an impulse with a long T_f and tens of oscillating frequency.

Figure 5 in [14] shows relationship of 50% breakdown voltage and gas pressure under standard LI and oscillating LI. In the range of 0.3-0.6 MPa, the 50% breakdown voltages of oscillating LI are higher than those of standard LI by 15.6%, 11.5%, 18.0% and 12.7% respectively. In other words, the local electric enhancement, like a particle defect, which can be detected by standard LI, may not be detected by oscillating LI.

The main differences between these two impulses are in the steepness of the wave and the oscillatory nature of the wave. Figure 6 shows the typical breakdown waveforms of SLI and OLI. Figure 7 shows the breakdown voltage as a function of time-to-breakdown under these two impulses. It is not hard to find that the breakdowns for oscillating LI almost occur in the front of the waveform, which is different for the standard LI with short T_f. Figure 8 shows relationship of 50% breakdown voltage and gas pressure under impulse with $T_f = 10$ μs and oscillating LI. The two impulses have a similar T_f and 50% breakdown voltage. Therefore, it can be inferred that the T_f plays an important role in

the insulation defect detecting effectiveness. The following research is focused on the effect of T_f.

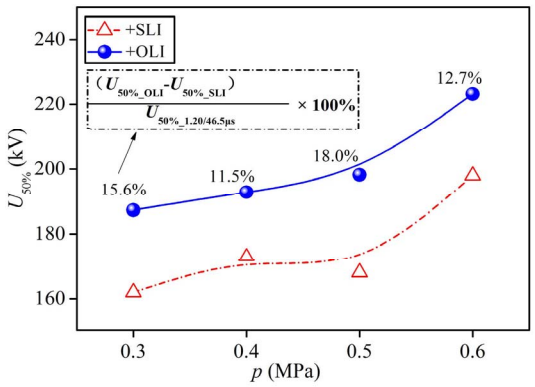

Figure 5. 50% breakdown voltage vs. gas pressure under standard LI and oscillating LI for 60 mm rod-plane gap [14].

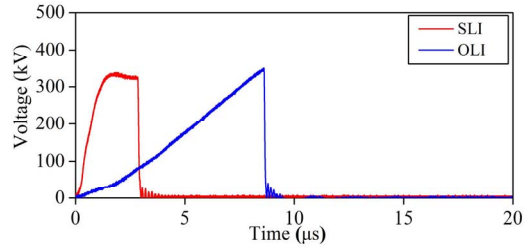

Figure 6. Typical breakdown waveforms of SLI and OLI.

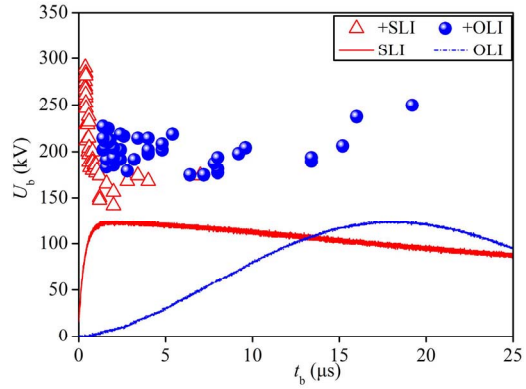

Figure 7. Breakdown voltage as a function of time-to-breakdown under standard LI and oscillating LI at an SF_6 pressure of 0.6 MPa for 60 mm rod-plane gap.

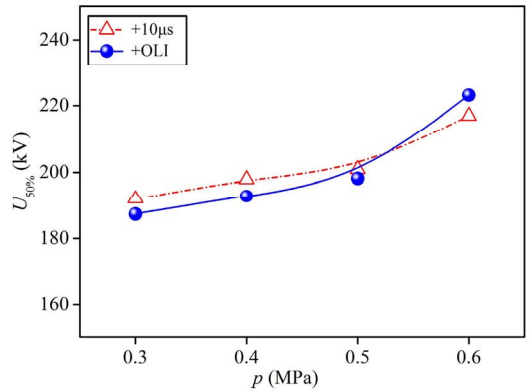

Figure 8. 50% breakdown voltage vs. gas pressure under impulse with T_f = 10 μs and oscillating LI for 60 mm rod-plane gap.

3.2 EFFECT OF WAVEFRONT TIME

Figure 9 shows the 50% breakdown voltage vs. double-exponential impulse wavefront times T_f in the range of 0.08 ~ 23.5 μs at 0.6 MPa for rod-plane gaps with different gap distance. It can be seen that with T_f increases, the 50% breakdown voltages have an increased trend. Especially when T_f exceeds 2.0 μs, the 50% breakdown voltage is higher than that of standard LI obviously.

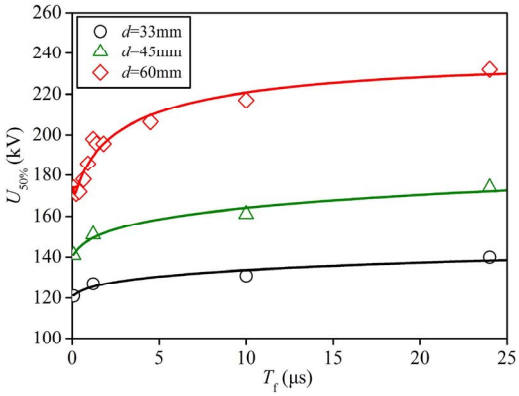

Figure 9. 50% breakdown voltage vs. double exponential impulse wavefront times T_f in the range of 0.08 - 23.5 μs at 0.6 MPa for rod-plane gaps.

Figure 10 shows the breakdown voltage as a function of time-to-breakdown under four different wavefront times 0.08, 1.2, 10 and 23.5 μs at an SF_6 pressure of 0.6 MPa for 33, 45 and 60 mm rod-plane gaps. Usually, the time-to-breakdown decreases with the increase of the breakdown voltage, as the trends for T_f=0.08, 1.2 μs. However, it is interesting to see that the time-to-breakdown increases with the increase of the breakdown voltage for T_f=10, 23.5 μs, which is opposite for the short T_f=0.08, 1.2 μs. Those points are experimental results. Based on the experimental data, the V-t curve can be fitted by

$$\log U_b = a + b\log t_b + c\left(\log t_b\right)^2 \quad (2)$$

where, U_b is the breakdown voltage in kV. t_b is the time to breakdown in μs. a, b, c are constants related to electrode structure and gas pressure. The fitting lines are shown by solid line in Figures 9. Equation (2) is undoubtedly suitable for highly inhomogeneous field in the test range. In Equation (2), a represents $\log U_b$ when t_b = 1 μs; $2c$ can represent the changing rate of the curve slope. Based on Equation (2), only three dates (U_b, t_b) can picture the V-t curve of the gas gap. In order to obtain an accurate curve, t_b of the dates should be distributed in a large range.

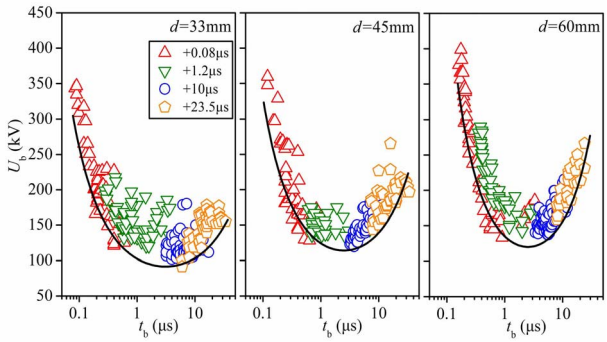

Figure 10. Breakdown voltage as a function of time-to-breakdown under four different wavefront times at an SF_6 pressure of 0.6 MPa for rod-plane gaps.

Another interesting phenomenon can be found that for T_f = 0.08 μs, the breakdowns all happen in the tail. But the breakdowns mostly occur in the front or near the peak for impulses with long T_f, especially when T_f = 10, 23.5 μs, which makes the breakdown voltage value is lower than the prospective voltage value. In order to further study the insulation defect detecting effectiveness, the Y-axis "Breakdown Voltage" of Figure 10 should be changed to "Prospective Voltage", as shown in Figure 11. The prospective voltage can be calculated by equation (1) for the breakdowns occur in the front. From Figure 11, it can be seen clearly that the minimum breakdown voltages U_{BDmin} increases with the increase of T_f (except for d = 33 mm), which can directly indicate that the insulation defects detecting effectiveness decreases with the increase of T_f from the point of the minimum breakdown voltages U_{BDmin}.

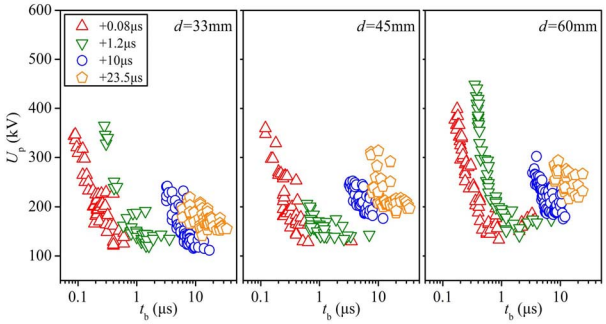

Figure 11. Prospective voltage as a function of time-to-breakdown under four different wavefront times at an SF_6 pressure of 0.6 MPa for rod-plane gaps.

3.3 EFFECT OF GAP DISTANCE

There is big difference in structure size of GIS for different voltage classes. The effect of gap distance should be considered in the research of detecting effectiveness. Figure 12 shows the standardized 50% breakdown voltage by SLI vs. double exponential impulse wavefront times T_f in the range of 0.08 - 23.5 μs at 0.6 MPa for 33, 45 and 60 mm rod-plane gap. Obviously, there is something different for the growth trend through careful comparison. It seems like that the trend for d = 60 mm grows fast than the others. The gap distance here also can reflect the field nonuniformity factor. Figure 13 shows the standardized 50% breakdown voltage by d = 33 mm vs. field nonuniformity factor f at 0.6 MPa for rod-plane gaps. For impulse with short T_f, with the increase of f, the $U_{50\%}/U_{50\%\_d=33mm}$ decreases faster than those impulses with long T_f.

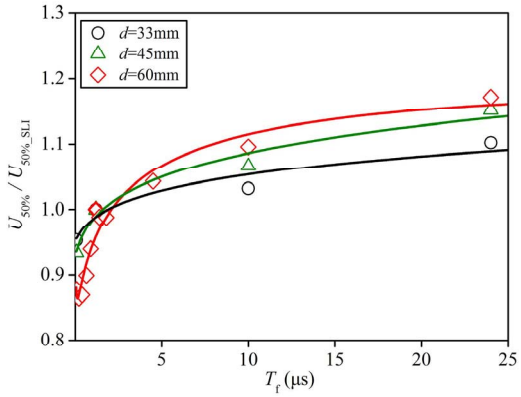

Figure 12. $U_{50\%}/U_{50\%\_SLI}$ vs. T_f in the range of 0.08 - 23.5 μs at 0.6 MPa for rod-plane gaps.

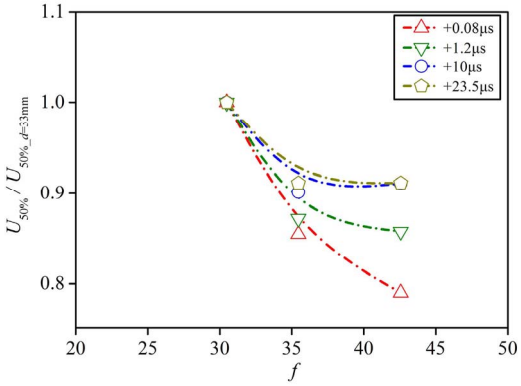

Figure 13. $U_{50\%}/U_{50\%\_d=33mm}$ vs. f at 0.6 MPa for rod-plane gaps.

Figure 14 shows the fitted V-t curves by Equation (2) at an SF_6 pressure of 0.6 MPa for 33, 45 and 60 mm rod-plane gaps. The values of empirical constants under different gap distances are shown in Table 2. From Figure 14, it can be seen that with the gap distance d increase, the rising part of the V-t curve is more obvious, especially for the right rising part when T_f is long. The phenomenon can also be verified from the value of 2c, which reflects the changing rate of the curve slope. And the flat part of the curve and the mouth of the U-shaped V-t curve become narrower.

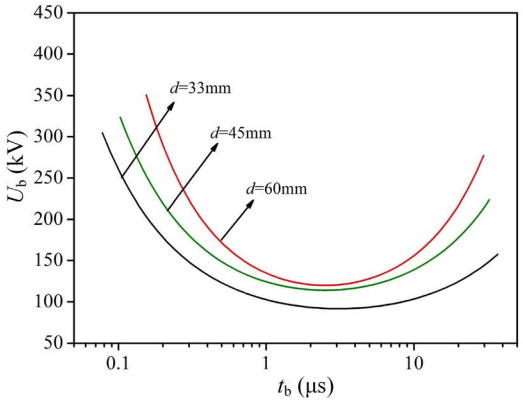

Figure 14. Fitted V-t curves at an SF_6 pressure of 0.6 MPa for 33, 45 and 60 mm rod-plane gaps.

Table 2. The values of empirical constants under different gap distances.

d/mm	a	b	c	2c
33	2.01	-0.20	0.20	0.40
45	2.09	-0.19	0.24	0.48
60	2.13	-0.25	0.32	0.64

3.4 EFFECT OF RISE RATE OF IMPULSE

For impulse with long T_f, the breakdowns almost occur in the front. The effect of T_f is the effect of the slope of impulse dU/dt essentially. The breakdown voltage U_b can has a relationship with the slope of impulse dU/dt, as shown in Figure 15. With the dU/dt increase, the U_b decreases. On one hand, for SF_6 highly inhomogeneous electric field, the discharge follows streamer/leader model. The displacement current flows through the streamer channel, which is induced by steep wavefront, injecting charges into streamer tip. The

charges build up at the streamer tip will enhance the electric field, which will promote the transformation of streamer to leader. For increasing impulse steepness, breakdown voltage will decrease from the viewpoint of the streamer to leader transition [17]. On the other hand, it can be explained by the effect of corona stabilization. Corona stabilization in SF_6 results in a delay of the discharge development and furthermore in an enhancement of the streamer inception and breakdown voltage. For impulse with low dU/dt, the changing rate of electric field E is low, under which the space charge can have an enough time to migration and diffusion before breakdown. The fully migration and diffusion of space charge can strengthen the shielding effect, and then increases the breakdown voltage. This can also explain the right rising part of the V-t curve. Meanwhile, for a settled (U_b, t_b), the prospective voltage value U_p can be calculated by Equation (1). Therefore, the longer the T_f, the higher the U_p. This trend can be found in Figure 11 for T_f = 10 and 23.5 μs.

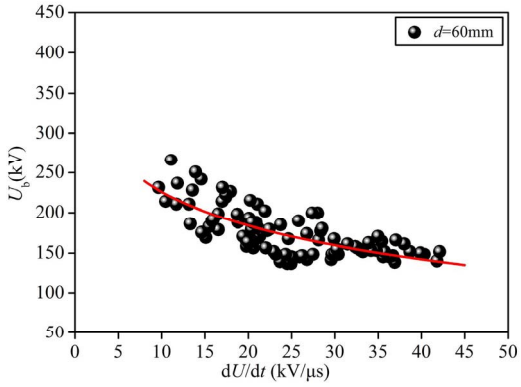

Figure 15. U_b vs. dU/dt at an SF_6 pressure of 0.6 MPa for 60 mm rod-plane gaps under T_f = 10, 23.5 μs.

At streamer or discharge inception, the area A in Figure 16 exceeds the critical value [15-16]. Then the critical volume V_{cr} becomes ionized, conducting and charged so that the internal field is reduced to almost E_{cr}, and the remaining ionization balances the drain of ions and electrons due to their field drift. Corona stabilization is caused by space charge formation ahead of the critical volume V_{cr}. Hence, the criterion for corona stabilization is simplified by the following condition [18].

$$v_I \geq v_{cr.m} \tag{3}$$

where, v_I is the ion velocity at the boundary of the critical volume, $v_{cr.m}$ is the maximum value of the growth velocity at the beginning.

$$v_I = \frac{b_I}{p}\left(\frac{E}{p}\right)_{cr} p = b_I\left(\frac{E}{p}\right)_{cr} = 620 \text{ m/s} \tag{4}$$

$$v_{cr.m} = x_{cr} = \frac{1}{2}\frac{E_m}{E_{cr}} r_t \tag{5}$$

where b_I is the field and pressure independent ion mobility. E_m is the changing rate of $E_m(t)$. Assuming the impulse as a beveled wave voltage, $E_m(t)$ can be written as $E_m(t) = E_m \cdot t$. Puting Equations (4) and (5) into the Equation (3), then the final criterion for corona stabilization is obtained:

$$E_m r \frac{1}{p} = \frac{dU}{dt} \cdot \frac{fr}{dp} \leq 109.65 \ \frac{\text{kV}}{\text{MPa} \cdot \mu\text{s}} \tag{6}$$

From Equation (6), it can be seen that the corona stabilization is not just in relationship with the rise rate of impulse, but also with electrode structure and gas pressure. For impulse with steep wavefront, the discharge process under certain conditions also exist corona stabilization. The phenomenon of "hump phenomenon" in the discharge of SF_6 gas in a highly inhomogeneous electric field is related to the distribution characteristic of space charge in the discharge process, and it can also reflect the corona stabilization effect in some degree.

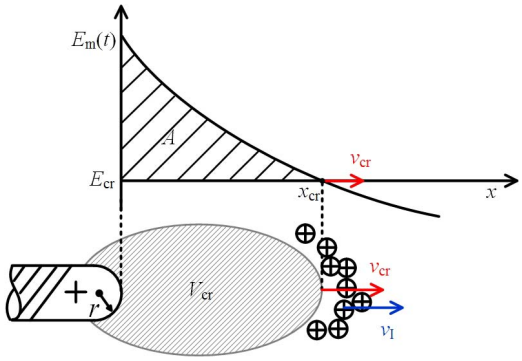

Figure 16. Streamer and field distribution at the tip of a rod.

Figure 17 shows relationship of 50% breakdown voltage and gas pressure of needle-plate electrodes under impulses with T_f = 0.08 μs and 15 μs. When T_f= 15 μs, L = 10 mm, the $U_{50\%}$-p curve has a significant hump phenomenon, indicating that there is an obvious corona stabilization. When decreasing T_f to 0.08 μs (T_f= 0.08 μs, L = 10 mm), the $U_{50\%}$-p curve does not show a hump phenomenon, as well as corona stabilization. However, when decreasing the length of the needle to L = 3 mm (T_f = 0.08 μs, L = 3 mm), which will also decrease the field nonuniformity factor f for the shielding effect of the GIS bus, the $U_{50\%}$-p curve shows a hump phenomenon, reflecting a certain corona stabilization effect. So the critical slope of impulse for corona stabilization (dU/dt)$_{cr}$ for different gaps can be calculated, as shown in Table 3. Figure 18 shows the dU/dt of impulses with different T_f for for 33, 45 and 60 mm rod-plane gaps. The picture indicates that the effect of corona stabilization occurs when T_f = 10 and 23.5 μs, and in some cases when T_f = 1.2 μs, but not occurs when T_f = 0.08 μs.

Figure 19 shows the effect of impulse slope for different gaps. For impulses with slopes of k_1 and k_2, the breakdown voltage has a difference ΔU. With the changing rate of the V-t curve increase, ΔU becomes bigger. Obviously, ΔU (d = 60 mm) > ΔU (d = 45 mm) > ΔU (d = 33 mm). Here, ΔU can reflect the sensitiveness of the gap breakdown voltage for dU/dt. Therefore, for SF_6 gaps with a longer gap distance d or a higher field nonuniformity factor f, the changing rate of the V-t curve is bigger, causing a bigger ΔU, which reflects that these gaps are more sensitive to dU/dt, also to T_f.

In a word, for ultra-high-voltage (UHV) GIS, which has a long gap distance, and where a defect may cause a more serious effect on electric field distribution, the changing rate

of the V-t curve slope is higher. That is to say the T_f of impulse has much more influence on the defect detecting effectiveness.

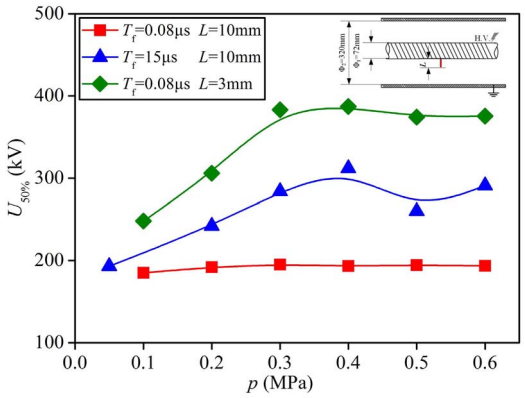

Figure 17. Relationship of 50% breakdown voltage and gas pressure of needle-plate electrodes under impulses with T_f= 0.08 μs and 15 μs.

Table 3. The critical slope of impulse for corona stabilization $(dU/dt)_{cr}$.

d/mm	p/MPa	r/mm	f	$(dU/dt)_{cr}$/kV·μs^{-1}
33	0.6	0.5	30.48	142
45			35.46	167
60			42.57	185

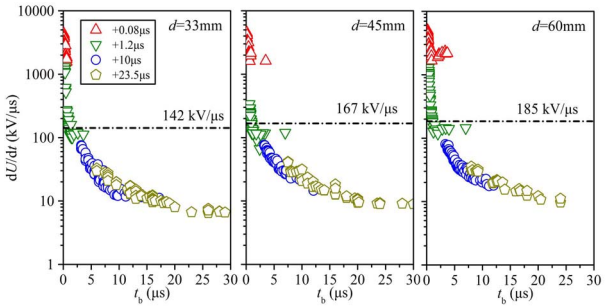

Figure 18. dU/dt of impulses with different T_f for for different gaps.

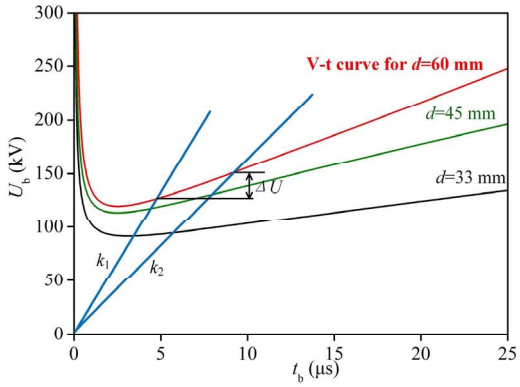

Figure 19. Effect of impulse slope on breakdown voltage for different gaps.

4 CONCLUSION

In order to evaluate the detecting effectiveness of on-site LI test for GIS equipment with insulation defects, based on the established multiple parameters impulse generating system, the insulation characteristics of SF_6 gas gap with highly inhomogeneous electric field under impulses with different waveform parameters were studied. These conclusions can be derived based on the experimental results.

(1) The insulation defects detecting effectiveness of oscillating LI with long T_f around 10 μs is lower than that of standard LI. According to the voltage-time characteristic, it can be inferred that the T_f plays an important role in the insulation defect detecting effectiveness. With T_f increases, the 50% breakdown voltages for rod-plane gaps have an increased trend.

(2) Prospective voltage is introduced to evaluate the insulation defects detecting effectiveness first. The insulation defect detecting effectiveness using the impulse test is reflected in the value of the prospective voltage. The prospective voltage-time characteristics confirm the conclusion that with the increase of impulse voltage T_f, the detection effectiveness for GIS insulation is reduced.

(3) The V-t curves of rod-plane gap under short T_f and long T_f present an opposite trend. The V-t curve shows a U-shaped in a wide range of t_b. The gap distance (or field nonuniformity factor) influences the shape of V-t curve. With the gap distance increase, the flat part of the curve and the mouth of the U-shaped V-t curve become narrower.

(4) The effect of T_f is the effect of the slope of impulse dU/dt essentially. SF_6 gaps with a higher field nonuniformity factor f are more sensitive to dU/dt, also to T_f. Corona stabilization effect is not just in relationship with the rise rate of impulse, but also with electrode structure and gas pressure. The critical dU/dt for corona stabilization is calculated for different rod-plane gaps.

ACKNOWLEDGMENT

This work was financially supported by the National Key R&D Program of China (2017YFB0903800) and Japan Power Academy.

REFERENCES

[1] Y. Li, Y. Shang, L. Zhang, R. Shi and W. Shi, "Analysis of very fast transient overvoltages (VFTO) from onsite measurements on 800 kV GIS", IEEE Trans. Dielectr. Electr. Insul., vol. 19, pp. 2102-2110, 2012.

[2] K. Srivastava and M. Morcos, "A review of some critical aspects of insulation design of GIS/GIL systems", in *Proceedings of IEEE PES Transmission and Distribution Conference and Exposition*, 2001, pp. 787-792.

[3] K. Tekletsadik and L. Campbell, "SF_6 breakdown in GIS," in Proceedings of IEE on Science, Measurement and Technology, pp. 270-276, 1996.

[4] A. Sabot, A. Petit and J. Taillebois, "GIS insulation co-ordination: on-site tests and dielectric diagnostic techniques, A utility point of view", IEEE Trans. Power Del., vol. 11, pp. 1309-1316, 1996.

[5] J. Meppelink, K. Diederich, K. Feser, et al, "Very fast transients in GIS", IEEE Trans. Power Del., vol. 4, pp. 223-233, 1989.

[6] N. Wiegart, L. Niemeyer, F. Pinnekamp, et al, "Inhomogeneous field breakdown in GIS-the prediction of breakdown probabilities and voltages. I. Overview of a theory for inhomogeneous field breakdown in SF_6", IEEE Trans. Pwr. Del., vol. 3, pp. 923-930, 1988.

[7] W. Chen, X. Yan, S. Wang, C. Wang, Z. Li, M. Dai, C. Li, W. Liu, H. Chen, Q. Zhang, G. Wei, and M. Zhang, "Recent progress in investigation on very fast transient overvoltage in gas insulated switchgear", Proc. CSEE, vo1. 31, pp. 1-11, 2011.
[8] U. Riechert and W. Holaus, "Ultra high-voltage gas-insulated switchgear-a technology milestone", Eur. Trans. Electr. Power, vol. 22, pp. 60-82, 2012.
[9] A. Pedersen, "On the electrical breakdown of gaseous dielectrics-an engineering approach," IEEE Trans. Dielectr. Electr. Insul., vol. 24, pp. 721-739, 1989.
[10] J. Laghari and A. Qureshi, "A review of particle-contaminated gas breakdown," IEEE Trans. Dielectr. Electr. Insul., vol. 16, pp. 388-398, 1981.
[11] High voltage switchgear and controlgear-Gas-insulated metal enclosed switchgear, IEC Standard 62271-203, 2003-11.
[12] Gas-insulated Metal-enclosed Switchgear for Rated Voltages of 72.5 kV and above, GB/T 7674, 2008.
[13] High-voltage test techniques-Part 1: General definitions and test requirements, IEC Standard 60060-1, 2010-09.
[14] T. Wen, Q. Zhang, Y. Qin, J. Zhao, J. Ma, Z. Wu, N. Shimomura, F. Tao, Y. Jia, Y. Yin, W. Shi and W. Chen, "On-site standard lightning impulse test for 1,100-kV gas-insulated switchgear with large capacitance", IEEE Electr. Insul. Mag., vol. 32, pp. 36-43, 2016.
[15] N.H. Malik and A.H. Qureshi, "Breakdown gradients in SF_6-N_2, SF_6-Air and SF_6-CO_2 Mixtures", IEEE Trans. Electr. Insul., vol. 15, pp. 413-418, 1980.
[16] T.W. Dakin, G. Luxa, G. Oppermann, J. Vigreux, G. Wind, H. Winkelkemper, "Breakdown of Gases in Uniform Fields", Electra, No 32, pp. 61-82, 1974
[17] Q. Zhang, L. Yang, Q. Chen, et al. The effect of impulse rising steepness on streamer to leader transition in non-uniform field gap in SF_6[J]. J. Appl. Phys. D: Applied Physics, 2003, 36 (10): 1212.
[18] T. Hinterholzer, W. Thomas and W. Boeck, "The influence of space-charge on the breakdown in SF_6", *Gaseous Dielectrics IX*, Springer US, pp. 383-389, 2001.

Tao Wen was born in Shaanxi Province, China, in 1990. He received the BS degree and Ph.D degree in electrical engineering from Xi'an Jiaotong University, Xi'an, China, in 2012 and 2017 respectively. He is currently a Post-doctor in the High Voltage Division, School of Electrical Engineering, and the State Key Laboratory of Electrical Insulation and Power Equipment, Xi'an Jiaotong University. He has also been working toward a doctoral double degree program at Tokushima University, Tokushima, Japan.

Qiaogen Zhang received the BS, MS, and PhD degrees in electrical engineering from Xi'an Jiaotong University, Xi'an, China, in 1988, 1991 and 1996 respectively. He is currently a professor in the High Voltage Division, School of Electrical Engineering, and the State Key Laboratory of Electrical Insulation and Power Equipment, Xi'an Jiaotong University. His major research interests include outdoor insulation, pulse power technology, gas discharge and its applications.

Jingtan Ma was born in Henan, China in 1993. He received the B.S. degree from Xi'an Jiaotong University, Shaanxi, China in 2014. He is currently working toward Ph.D. degree at the High Voltage Division, School of Electrical Engineering, and the State Key Laboratory of Electrical Insulation and Power Equipment.

Xuandong Liu was born in Sichuan, China, in 1981. He received the B.S. degree in automation from the Chongqing University of Post and Telecommunication, Chongqing, China, in 2004, and the Ph.D. degree from Xi'an Jiaotong University, Xi'an, China, in 2011. He is currently an Associate Professor with the State Key Laboratory of Electrical Insulation and Power Equipment, Xi'an Jiaotong University.

Zhicheng Wu was born in Yunnan, China in 1993. He received the B.S. degree from the Xi'an Jiaotong University, Shaanxi, China in 2015. He is currently working toward the PhD degree in the High Voltage Division, School of Electrical Engineering, and the State Key Laboratory of Electrical Insulation and Power Equipment.

Lingli Zhang was born in Jiangsu, China in 1992. She received the B.S. degree from Xi'an Jiaotong University, Shaanxi, China in 2015. She is currently a postgraduate student at the High Voltage Division, School of Electrical Engineering, and the State Key Laboratory of Electrical Insulation and Power Equipment. She is now engaged in the research of GIS insulation features.

Junping Zhao received the B.S. degree in applied physics from the University of Science and Technology of China, Hefei, China, in 2001, the M.S. degree in nuclear technology and application from China Academy of Engineering Physics, Mianyang, China, in 2004, and the Ph.D. degree in electrical engineering from Xi'an Jiaotong University, Xi'an, China, in 2013. He is currently an associate professor with the High Voltage Division, School of Electrical Engineering, and the State Key Laboratory of Electrical Insulation and Power Equipment, Xi'an Jiaotong University, Xi'an, China.

Naoyuki Shimomura (M'97) was born in Fukuoka, Japan. He received the B.E., M.E. and Dr. Eng. degrees from Kumamoto University, Kumamoto, Japan, in 1987, 1989, and 1996 respectively. Since 1990, he has been with Tokushima University, Tokushima, Japan, first as a Research Associate and currently as a Professor. During 1997-1998, he was on sabbatical leave with the University of New Mexico, Albuquerque, and the Air Force Research Laboratory, Albuquerque. His research interests include pulsed power applications as improvement of environment and bioelectrics.

Weijiang Chen was born in Shan Dong Province, China, in 1958. He received the B.S. degree in electrical engineering from HeFei University of Technology, Hefei, China, in 1982. He received the M.S. degree in high voltage and insulation from China Electric Power Research Institute, Beijing, China, in 1985. He is currently a professor with the Ultra High Voltage Department, State Grid Corporation of China.